Available online at www.sciencedirect.com
ScienceDirect
Trans. Nonferrous Met. Soc. China 35(2025) 965−974
Transactions of Nonferrous Metals Society of China
www.tnmsc.cn

In-situ reduction mechanism of hematite by bastnaesite during suspension magnetization roasting

Wen-bo LI[1,2], Shao-kai CHENG[1,2], Rui QU[1,2], Ji-jia CHEN[1,2]

1. School of Resources and Civil Engineering, Northeastern University, Shenyang 110819, China;
2. National-Local Joint Engineering Research Center of High-Efficient Exploitation Technology for Refractory Iron Ore Resources, Shenyang 110819, China

Received 31 July 2023; accepted 21 March 2024

Abstract: To explore the spontaneous magnetization of iron-bearing rare earth ores during suspension roasting, binary minerals containing hematite and bastnaesite were used to investigate the effects of the roasting temperature, roasting time, and bastnaesite-to-hematite mass ratio on in-situ reduction of hematite in a N_2 atmosphere. Relevant analytical tests were used to explore the mineral phase evolution during roasting, the magnetism and microstructure of the roasted products, the phase composition, and the surface element valence of concentrate. It was found that magnetic separation of the iron concentrate afforded an iron grade of 68.87% and a recovery of 93.18% under the optimum roasting conditions. During roasting, bastnaesite decomposed to generate CO_2 and CO, and the compact structure of hematite was gradually destroyed, resulting in microcracks. Subsequently, the CO entered the surface of the hematite through the microcracks and reacted to form a magnetite shell, and the magnetite-encapsulated hematite particles were recovered via low-intensity magnetic separation.

Key words: bastnaesite; hematite; magnetization roasting; in-situ reduction

1 Introduction

Rare earth elements (REEs) are widely used in electronics, manufacturing, medicine, and national defense due to their unique physicochemical properties [1−3]. In the transition from modern industry to a green economy, REEs have become particularly valuable [4,5]. REEs typically exist in nature as carbonates and phosphates and coexist with other minerals [6,7]. Due to the differences in specific gravity, magnetic property, electrical conductivity, and floatability of rare earth minerals and their associated minerals, beneficiation processes are usually used to produce high-grade rare earth minerals with rare earth oxide (REO) contents of 50−60 wt.%, which can reduce the energy and reagent consumption in metallurgical processes [8−10].

Large iron-bearing rare earth deposits are present in China, Australia, and Canada, but due to the complex ore structures, conventional beneficiation processes fail to separate the iron and rare earth minerals effectively [11]. For example, the iron and rare earth minerals in the Bayan Obo deposit are enriched mainly through "low/high-intensity magnetic separation–flotation", which, however, suffers from the loss of valuable minerals and the inability to efficiently separate low-grade refractory ores [2,12,13]. Magnetization roasting is considered an efficient pretreatment method for enriching low-grade weakly magnetic iron minerals [14−16].

Corresponding author: Wen-bo LI, Tel: +86-15840380911, E-mail: liwenbo@mail.neu.edu.cn;
Shao-kai CHENG, Tel: +86-15263733082, E-mail: 2110409@stu.neu.edu.cn
DOI: https://doi.org/10.1016/S1003-6326(24)66727-0

Researchers have proposed enhancing the magnetic difference between iron minerals and rare earth minerals through magnetization roasting, and then concentrating the iron minerals in the roasted products by magnetic separation and recovering the high-content rare earth minerals in the tailings by flotation [17]. YANG et al [18] pretreated Bayan Obo iron-containing rare earth tailings by coal-based magnetization roasting and obtained a magnetic separation concentrate with an iron grade of 45.45% and an iron recovery of 68.36% through low-intensity magnetic separation. FARIS et al [19] studied the factors affecting the transformation of goethite to magnetite during magnetization roasting for ferruginous rare earth-bearing lateritic ore in Australia and determined the optimum roasting temperature range to be 600−650 °C. In addition, they found that monazite remained stable during roasting.

Our previous [20] research found that magnetization roasting with hydrogen as a reducing agent resulted in excellent iron separation, and following rare earth flotation tests proved that roasting did not adversely affect the recovery of rare earth minerals. Moreover, it was found that the in-situ (no reductant added) magnetization roasting process also yielded an iron concentrate with an iron grade of 60.44% and an iron recovery of 76.04%. The presence of bastnaesite during roasting allowed the conversion of hematite to magnetite without the addition of a reducing agent.

In response to the magnetization of hematite under a N_2 atmosphere, the reaction and mechanism for in-situ reduction of hematite were explored by bastnaesite. Initially, the effects of the roasting temperature, roasting time, and bastnaesite-to-hematite mass ratio on the in-situ reduction of hematite were investigated with a mixed system of bastnaesite and hematite. The mineral phase evolution and changes in microstructure and surface properties during roasting were analyzed via in situ X-ray diffraction (XRD), vibrating sample magnetometry (VSM), scanning electron microscopy equipped with energy dispersive spectroscopy (SEM–EDS), Mössbauer spectroscopy, and X-ray photoelectron spectroscopy (XPS). Based on the analytical tests, a mechanism model was established for in-situ reduction of hematite by bastnaesite during roasting. This study is informative for clean magnetization roasting of iron-bearing rare earth ores.

2 Experimental

2.1 Materials

The single minerals of hematite and bastnaesite used in the test were taken from the Baogang Group, China. The particle sizes of the prepared single minerals ranged from 37 to 74 μm to ensure be well-suspended. The chemical compositions and XRD patterns of the samples are shown in Table 1 and Fig. 1, respectively. The contents of REO, F and C in the bastnaesite samples were 69.40%, 8.50% and 5.29%, respectively, and the contents of TFe and FeO in the hematite samples were 67.82% and 0.72%, respectively. No miscellaneous peaks were found in the XRD patterns of the two minerals. Therefore, the samples met the test requirements.

Table 1 Chemical compositions of hematite and bastnaesite samples (wt.%)

Mineral	TFe	FeO	CaO	SiO_2	Al_2O_3	S	P
Hematite	67.82	0.72	0.19	0.74	0.31	0.01	0.04
Mineral	REO	F	C	Ba	S	P	LOI
Bastnaesite	69.40	8.50	5.29	0.27	0.19	0.03	18.28

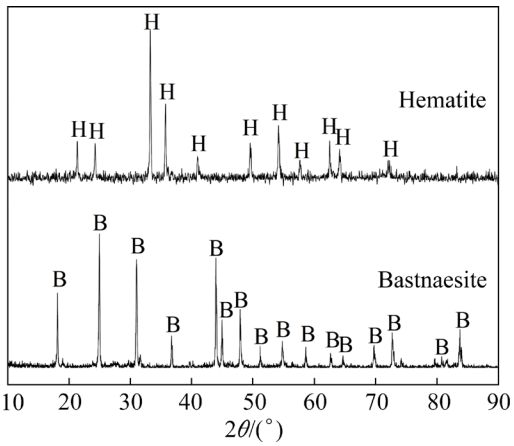

Fig. 1 XRD patterns of hematite and bastnaesite samples

2.2 Methods

2.2.1 Experimental procedure

The reduction of hematite by bastnaesite and its mechanism were explored by suspension roasting. The test flow chart is shown in Fig. 2. The bastnasite and hematite were mixed in a certain proportion, and 15 g of the mixed ores was weighed and placed in a quartz tube in the vertical roasting furnace (OTF−1200X-S-VT). N_2 was continuously

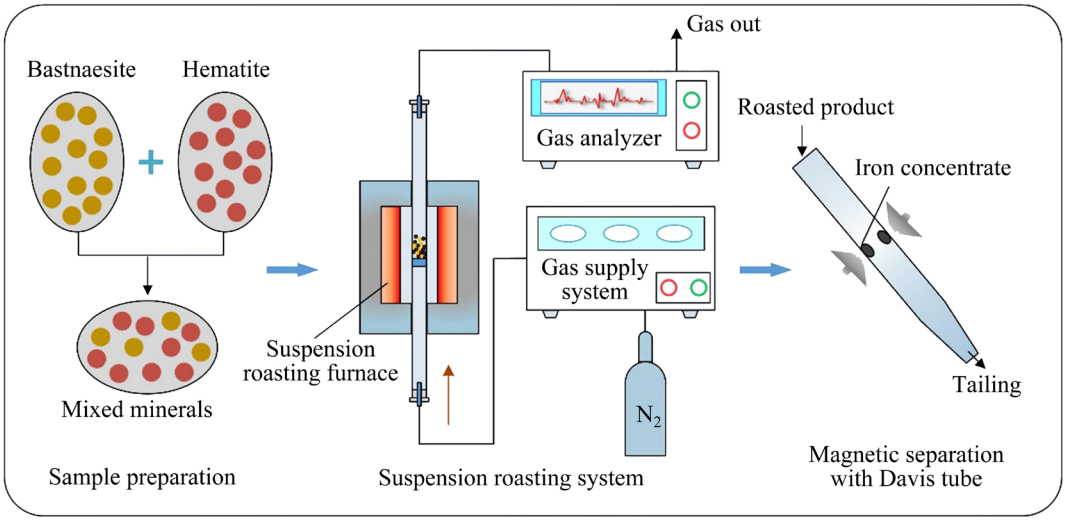

Fig. 2 Schematic diagram of test process flow

fed into the furnace to keep the particles suspended during roasting. To evaluate the reduction of hematite by bastnaesite, a Davis tube tester (CXG50) was used to treat the roasted products (magnetic field intensity: 107 kA/m, duration: 3 min). The iron grade and iron recovery of the magnetic separation concentrate were used as evaluation indices for in-situ reduction of hematite induced by bastnaesite. The recovery of the iron concentrate was calculated as

$$\varepsilon = \frac{m_1\beta}{m_2\alpha} \times 100\% \quad (1)$$

where ε is the iron concentrate recovery, β is the iron concentrate grade, α is the iron grade of the feed, m_1 is the mass of the concentrate, and m_2 is the mass of the feed.

2.2.2 Analytical test

An X-ray diffractometer (PANalytical Empyrean) was used for in-situ detection of the phase evolution during roasting. The test temperature range was 400−800 °C, the heating rate was 50 °C/min, the test interval was 50 °C, and the angular scan rate was 15 °C/min. Subsequently, the magnetic and microstructural evolution of the roasted products were investigated with a vibrating sample magnetometer (VSM, JDAW−2000D) and scanning electron microscopy-energy dispersive spectroscopy (SEM–EDS, SSX−550), respectively. In addition, a Mössbauer spectrometer (MFD−500AV−02) and an XPS system (Thermo Scientific K_α) were used to explore the phase composition and surface element valence states of the magnetic separation concentrate.

2.2.3 Thermodynamic analysis

The thermodynamic data for common compounds can be obtained by referring to the thermodynamic table; however, due to the difficulty in obtaining pure minerals containing rare earths (e.g., $RECO_3F$, REOF, etc.), the thermodynamic data for these rare earth compounds are not available. In this case, the group contribution method developed can be used to estimate the standard enthalpy of formation $\Delta_f H^{298}$, the standard Gibbs free energy of formation $\Delta_f G^{298}$, and the isobaric heat capacity C_p [21−24]. Cerium (Ce) is the dominant element in bastnaesite, and Ce was used to denote the REEs throughout this work. Under a N_2 atmosphere, the reactions that occur in the system are shown by Eqs. (2) to (5). According to the group contribution method, $CeCO_3F$, CeOF and Ce_7O_{12} are composed of Ce^{3+}, Ce^{4+}, F^-, CO_3^{2-}, and O^{2-}. The contributing factors of the groups and the contribution values of the correlation coefficients are shown in Table 2, and the thermodynamic data for the other compounds are from BARIN [25]. Then, the reaction enthalpy $\Delta_r H(T)$ and the reaction Gibbs free energy $\Delta_r G(T)$ are obtained from the Kirchhoff equation and Van't Hoff equation [21−24].

$$CeCO_3F(s)=CeOF(s)+CO_2(g) \quad (2)$$

$$21CeOF(s)+3CO_2(g)=2Ce_7O_{12}(s)+7CeF_3(s)+3CO(g) \quad (3)$$

$$Ce_7O_{12}(s)+2CO_2(g)=7CeO_2(s)+2CO(g) \quad (4)$$

$$3Fe_2O_3(s)+CO(g)=2Fe_3O_4(s)+CO_2(g) \quad (5)$$

Table 2 Contributions of groups for $\Delta_f H^{298}$, $\Delta_f G^{298}$ and C_p [23,24]

Group	ΔH_j/(kJ·mol^{-1})	ΔG_j/(kJ·mol^{-1})	Δa_j	Δb_j	Δc_j	Δd_j
Ce^{3+}	−716.558	−569.967	13.011	−7.089	0.762	4.687
Ce^{4+}	−741.400	−564.929	8.506	−6.387	0.734	8.045
CO_3^{2-}	−616.496	−635.990	47.278	86.757	−0.887	−5.133
F^-	−310.918	−326.667	22.041	15.652	−0.244	1.538
O^{2-}	−173.650	−229.836	28.152	12.043	−0.747	−4.023

ΔH_j and ΔG_j are the contribution factors for $\Delta_f H^{298}$ and $\Delta_f G^{298}$, and Δi_j (i=a, b, c, d) is the correlation coefficient for C_p

Figure 3 shows the thermodynamic results from the above equations. As shown in Fig. 3, roasting will cause the decomposition of $CeCO_3F$ to generate CeOF and CO_2 (Eq. (2)), and the reaction trend is more pronounced at higher temperatures. $\Delta_r G(T)$ in Eq. (3) is negative, which indicates that CeOF and CO_2, the thermal decomposition products of bastnaesite, react with each other to produce Ce_7O_{12} and CO. When the temperature exceeds 417 °C, Ce_7O_{12} is further oxidized to CeO_2 with the formation of CO (Eq. (4)). Furthermore, CO acts as the reducing agent to convert hematite to magnetite (Eq. (5)). The thermodynamic analysis shows that bastnasite reduces hematite in situ; however, these results can indicate only the possibility of spontaneous reactions, and the actual process must be explored further.

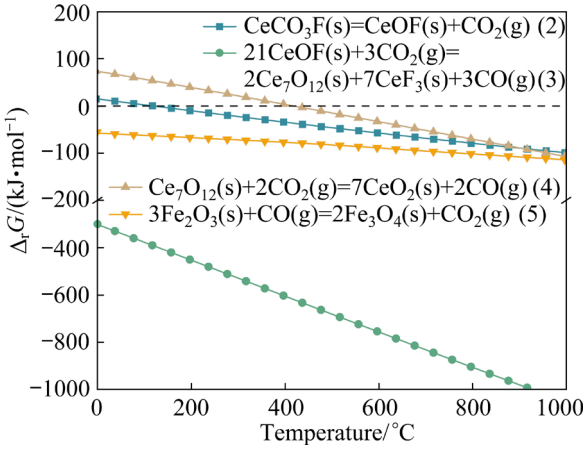

Fig. 3 Relationship between Gibbs free energy change and temperature of Eqs. (2)−(5)

3 Results and discussion

3.1 In-situ magnetization roasting–magnetic separation test

3.1.1 Effects of roasting temperature

Figure 4 shows the effects of the roasting temperature on the indices for the magnetic separation

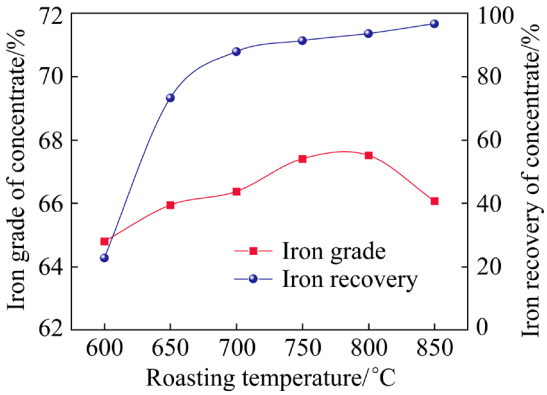

Fig. 4 Effects of roasting temperature on indices for magnetic separation

concentrate with a roasting time of 10 min and a bastnaesite-to-hematite mass ratio of 1:2. As the roasting temperature was increased to 800 °C, the iron grade gradually increased to 67.51%. However, when the temperature continued to increase to 850 °C, the iron grade tended to decrease. This occurred because the roasted products of bastnaesite were eroded on the surfaces of the iron mineral particles at high temperatures, resulting in a decrease in the iron grade of the concentrate. In the temperature range 600−700 °C, the iron recovery increased rapidly, while the increasing trend became slower after the temperature exceeded 700 °C. It is speculated that only a small amount of hematite was reduced because less CO gas was generated by the decomposition of bastnaesite at lower temperatures. In summary, 800 °C was selected as the optimal roasting temperature for continued exploration of the effects of roasting time and the bastnaesite-to-hematite mass ratio.

3.1.2 Effects of roasting time

The effects of the roasting time on the magnetic separation indexes were investigated at a roasting temperature of 800 °C and a bastnaesite-to-hematite mass ratio of 1:2, and the results are presented in Fig. 5. When the roasting time was

between 4 and 13 min, the iron grade and iron recovery fluctuated slightly, and the fluctuation ranges were 67.95%−68.87% and 91.22%−93.18%, respectively. However, when the roasting time was less than 4 min, the iron grade was high, but the iron recovery was extremely low. This indicated that since the extent of bastnaesite thermal decomposition degree was low in this relatively short period, it did generate enough CO to promote the reduction of hematite, and the magnetic separation concentrate had a very small amount of high-grade hematite. To leave enough time for the thermal decomposition of bastnaesite, the roasting time was determined to be 4 min.

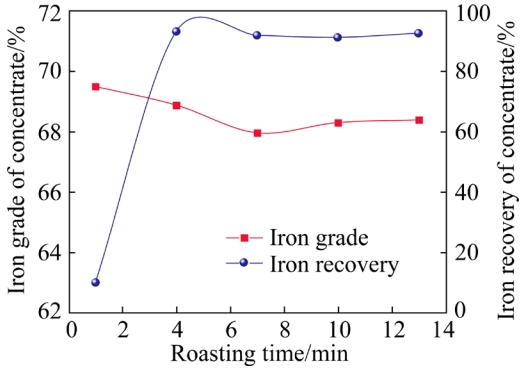

Fig. 5 Effects of roasting time on magnetic separation indices

3.1.3 Effects of bastnaesite-to-hematite mass ratio

By fixing a roasting temperature of 800 °C and a roasting time of 4 min, the effects of the bastnaesite-to-hematite mass ratio on the magnetization roasting process were explored. The test results are shown in Fig. 6. With the increase in the bastnaesite-to-hematite mass ratio, the iron grade of the concentrate was stable at approximately 69%, and the iron recovery showed a trend of increasing sharply at first and then increasing slowly. When the bastnaesite-to-hematite mass ratio was increased from 3:10 to 5:10, the iron recovery increased rapidly from 77.71% to 93.18%; then, as the bastnaesite-to-hematite mass ratio was increased further, the iron recovery increased slowly, from 93.18% to 96.11%. Based on the above analysis, under suitable roasting conditions (a roasting temperature of 800 °C, a roasting time of 4 min, and a bastnaesite-to-hematite mass ratio of 1:2), CO generated by the decomposition of bastnaesite has an excellent reducing effect on hematite, promoting the recovery of iron minerals.

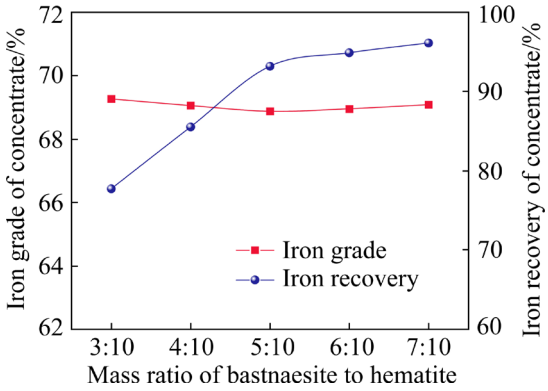

Fig. 6 Effects of bastnasite-to-hematite mass ratio on magnetization roasting

3.2 Phase transitions during roasting

To further explore the phase transition pattern of the mixed system of bastnaesite and hematite, in-situ XRD was performed at high temperatures under a N_2 atmosphere. The XRD spectra are shown in Fig. 7. When the temperature was lower than 450 °C, the XRD diffraction peaks did not change. When the temperature ranged from 450 to 700 °C, the diffraction peak intensity changed, but no new phase was detected. The diffraction peaks of magnetite began to appear when the temperature exceeded 700 °C, which explains the low iron recovery at roasting temperatures below 700 °C in Fig. 4. The diffraction peaks of CeOF also first appeared when the roasting temperature exceeded 700 °C, but notably, they shifted to higher angles, which was due to the oxidation of CeOF [26]. When the roasting temperature was 800 °C, the diffraction peak corresponding to $CeCO_3F$ disappeared completely, which indicated that the bastnaesite was completely decomposed. In addition, a comparative experiment involving roasting of the bastnaesite monomineral (5 g) was designed, and the gas-phase products produced by roasting were monitored in real-time with a gas analyzer, which detected CO during the roasting of bastnaesite. The CO flow rates are shown in Fig. 8. As the temperature was increased from 600 to 800 °C, the instantaneous flow rate of the CO produced from roasting of bastnaesite continued to increase. When the temperature was below 600 °C, no CO was detected. This indicated that in the mixed system of bastnaesite and hematite, the thermal decomposition of bastnaesite generated CO, which then reduced the hematite to magnetite.

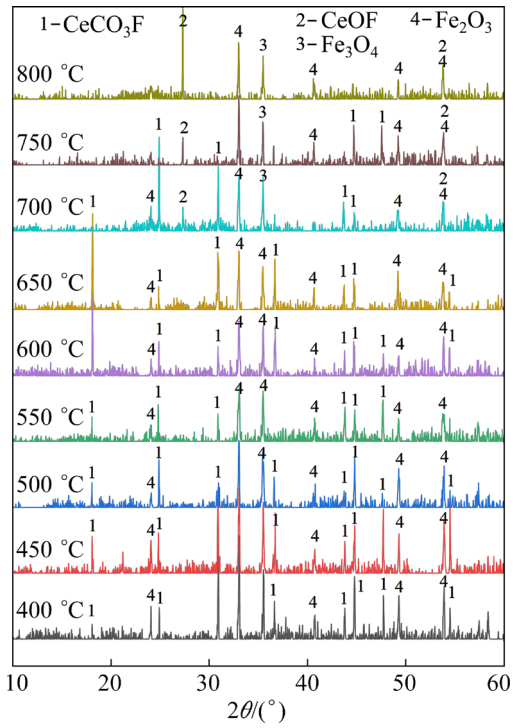

Fig. 7 In-situ XRD patterns of bastnaesite−hematite system at different temperatures

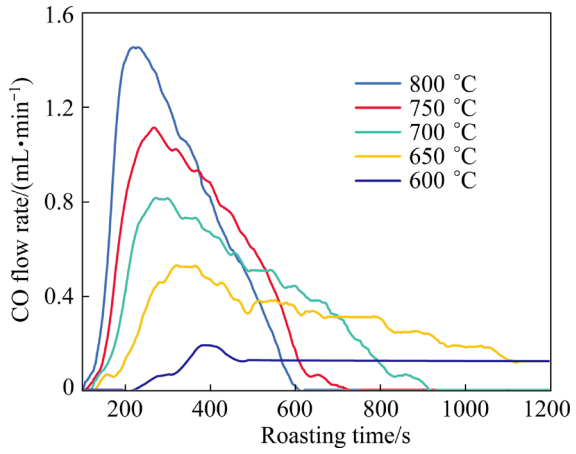

Fig. 8 Real-time flow rate of CO during roasting of bastnaesite

3.3 Characteristic analysis of roasted products

The magnetic properties of the mixed bastnaesite and hematite before and after roasting were analyzed using VSM, as shown in Fig. 9. The specific magnetic susceptibility of the roasted products increased with increasing magnetic field intensity and eventually reached saturation (14.50 $A \cdot m^2 \cdot kg^{-1}$). Compared with the saturation specific magnetic susceptibility of the sample before roasting (1.56 $A \cdot m^2 \cdot kg^{-1}$), that of the roasted products was much greater [27,28]. This indicated that the decomposition of bastnaesite induced the reduction of hematite.

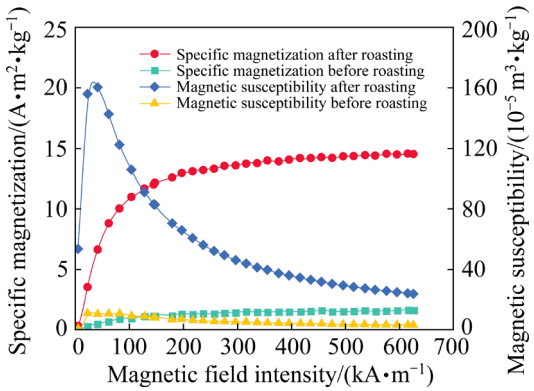

Fig. 9 Magnetic analysis of roasted product

In addition, SEM–EDS was used to analyze the microstructure of the roasted product, which was compared with those of the samples roasted at different time. The results are shown in Fig. 10. Before roasting, the mixed ore had a smooth and compact structure with no obvious cracks (Fig. 10(a)). With prolongation of the roasting time, the bastnaesite thermally decomposed from the outer layer to the inner layer, resulting in cracks pointing to the particle center (Fig. 10(b)). The EDS spectra showed that bastnaesite decomposed to generate CeOF (Fig. 10(e)). After the bastnaesite was completely decomposed into CeOF (Fig. 10(f)), the particle structure was disrupted. The dense pores and cracks were caused by the gas generated during the decomposition of bastnaesite (Fig. 10(c)). Moreover, the surfaces of the hematite particles reacted with CO generated by the decomposition of bastnaesite to form magnetite (Figs. 10(d) and (f)). The newly formed magnetite wrapped around the hematite to form an outer layer, and the inner layer was still hematite. The magnetite shell encapsulating the hematite was the reason for efficient magnetic capture of the iron minerals in the roasted products.

3.4 Characteristics analysis of magnetic separation concentrate

To explore the phase composition of iron in the roasting−magnetic separation concentrate, Mössbauer spectroscopy was performed, and the results are shown in Fig. 11 and Table 3. As shown in Fig. 11, the Mössbauer spectrum comprised three sets of 6-peak subspectra (named subspectrum 1, subspectrum

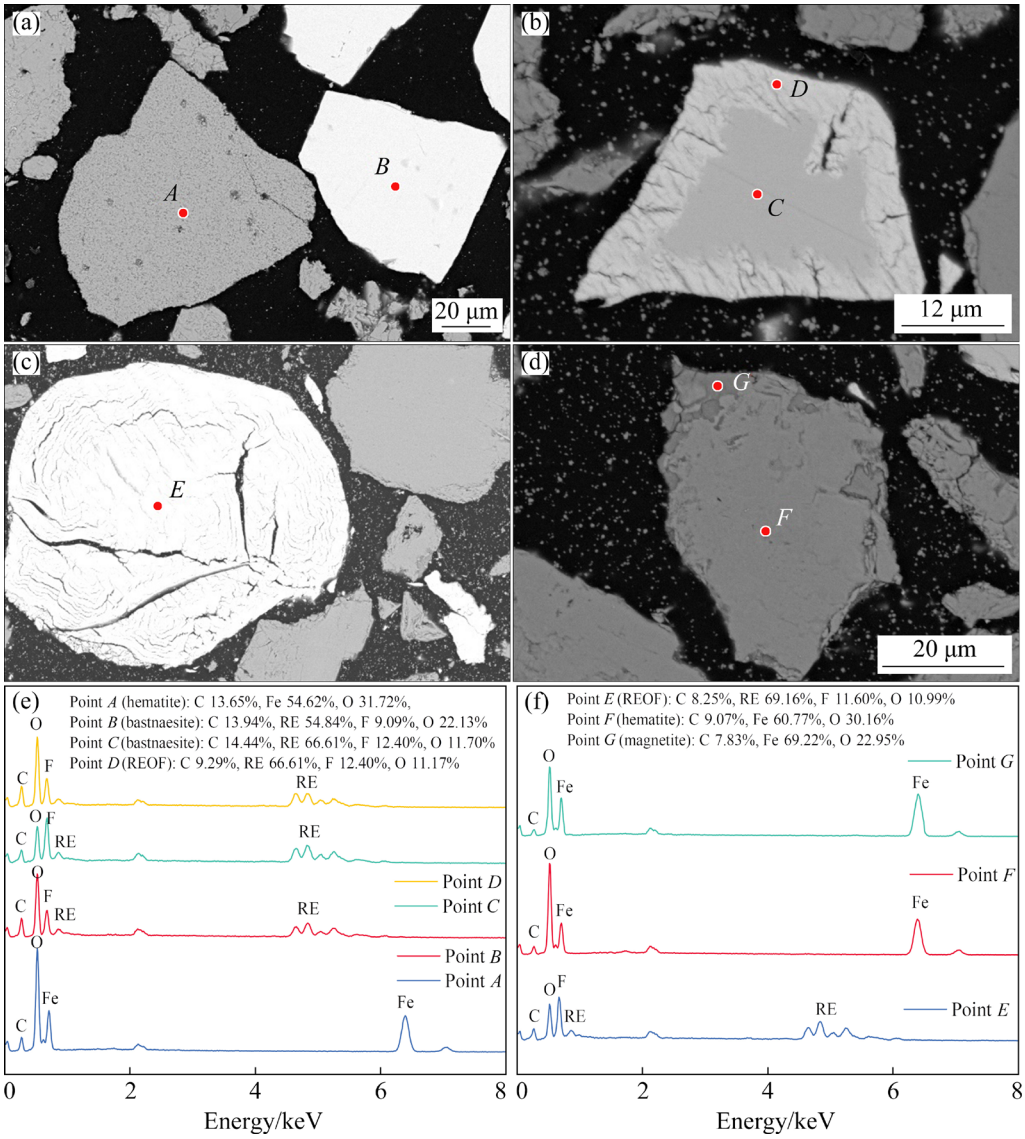

Fig. 10 Microstructures and EDS spectra of products roasted at different time: (a) Unroasted; (b) Roasting for 1 min; (c) Bastnaesite particles roasting for 4 min; (d) Iron ore particles roasting for 4 min; (e) EDS spectra of Points *A* to *D*; (f) EDS spectra of Points *E* to *G*

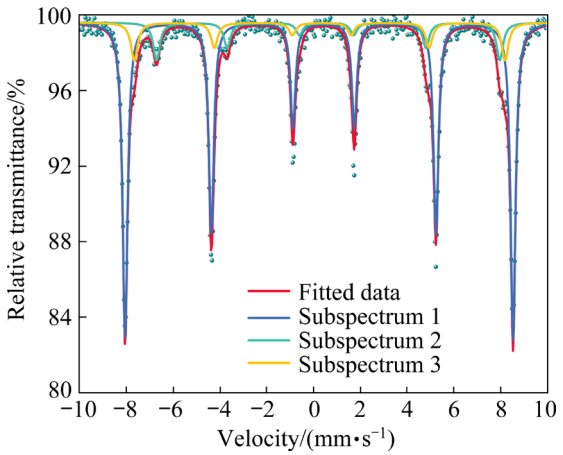

Fig. 11 Musburger spectra of magnetic separation concentrate

2, and subspectrum 3). Subspectrum 1 (IS= 0.371 mm/s, QS=−0.196 mm/s) was attributed to Fe^{3+} in hematite; Subspectrum 2 (IS=0.343 mm/s, *H*=49.33 T) and Subspectrum 3 (IS=0.629 mm/s, *H*=45.66 T) correspond to the Fe^{3+} at tetrahedral positions and $Fe^{2.5+}$ at the octahedral position in magnetite, respectively [29]. Obviously, the magnetic separation concentrate was composed of weakly magnetic hematite (75.8%) and strongly magnetic magnetite (24.2%).

Figure 12 shows the XPS spectra of the magnetic separation concentrate and hematite. In Fig. 12(a), the binding energy of the Fe $2p_{3/2}$ photoelectron peak was 711.40 eV, and the binding

energy of the Fe $2p_{1/2}$ photoelectron peak was 724.00 eV. Both peaks corresponded to Fe^{3+}—O bonds, which shows that Fe on the surface of hematite mainly existed as Fe^{3+} and in the form of Fe_2O_3. With increasing magnetic separation concentration (Fig. 12(b)), the Fe 2p peak significantly shifted, and the Fe $2p_{3/2}$ and Fe $2p_{1/2}$ photoelectron peaks corresponded to Fe^{2+} — O bonds, which indicated that Fe on the surface of the magnetic separation concentrate mainly existed as Fe^{2+} and in the form of Fe_3O_4. Comparing the areas of Fe^{3+} and Fe^{2+} photoelectron peaks in the hematite and magnetic separation concentrate, samples revealed that the photoelectron peak area of Fe^{3+} in hematite was larger than that in the magnetic separation concentrate, whereas the photoelectron peak area of Fe^{2+} in the magnetic separation concentrate was larger than that in hematite. These results indicate that Fe^{3+} was reduced to Fe^{2+} during the roasting process [30,31].

3.5 Reaction mechanism model

Based on the above tests and detection analysis results, a mechanism model through which bastnaesite induces the in-situ reduction of hematite in suspension magnetization roasting of hematite is proposed, as shown in Fig. 13. With increasing temperature, the bastnaesite thermally decomposed to generate CO_2 and CO. Additionally, the compact structure of hematite was gradually destroyed, resulting in pores and microcracks. CO entered the surfaces of the hematite particles through pores and

Table 3 Analytical parameters of Musburger spectra of magnetic separation concentrate

Subspectrum	IS/(mm·s^{-1})	QS/(mm·s^{-1})	*H*/T	Subspectrum area/%
1	0.371	−0.196	51.62	75.8
2	0.343	−0.090	49.33	12.3
3	0.629	0.070	45.66	11.9

IS: Isomer shift; QS: Quadrupole splitting; *H*: Magnetic field

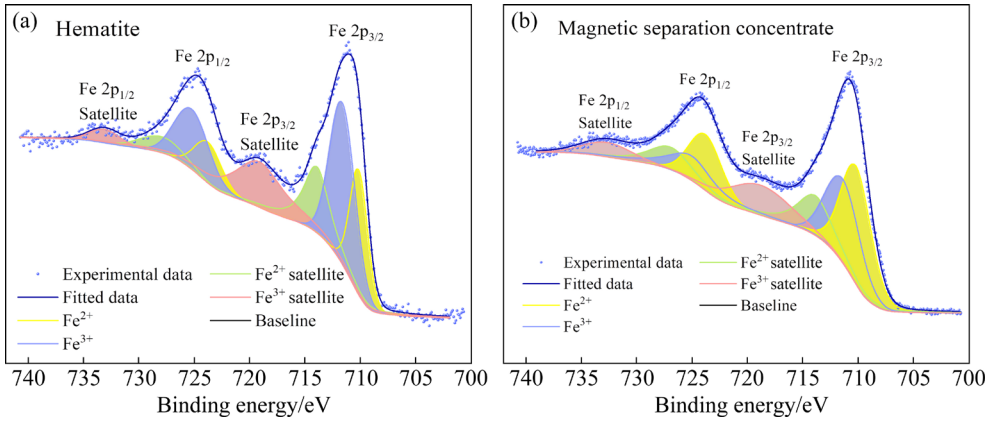

Fig. 12 XPS spectra of hematite (a) and magnetic separation concentrate (b)

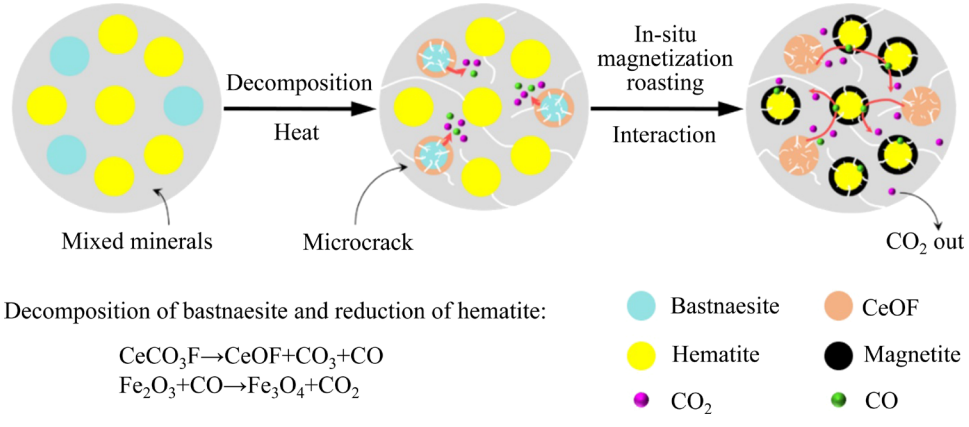

Fig. 13 Schematic diagram of roasting reaction mechanism of mixed sample of hematite and bastnaesite

microcracks and reduced the surface hematite to magnetite. Finally, the bastnaesite completely decomposed into CeOF, and the hematite particles were transformed into encapsulated particles in which the magnetite shell wrapped the inner hematite.

4 Conclusions

(1) The optimal conditions for in situ magnetization roasting of a mixture of hematite and bastnaesite included a roasting temperature of 800 °C, a roasting time of 4 min, and a bastnaesite-to-hematite mass ratio of 1:2. The roasted product was separated by magnetic separation to obtain a concentrate with an iron grade of 68.87% and an iron recovery of 93.18%.

(2) During the roasting process, the thermal decomposition products of bastnaesite were CeOF, CO_2 and CO, and some part of the hematite was transformed into magnetite. Roasting increased the saturation specific magnetic susceptibility of the mixed sample from 1.56 to 14.50 $A \cdot m^2 \cdot kg^{-1}$. This occurred because CO generated by the decomposition of bastnaesite reacted with the surface layers of the hematite particles to form a magnetite shell.

(3) The hematite-to-magnetite mass ratio of the magnetic separation concentrate was approximately 3:1, but the surface Fe mainly existed in the form of Fe^{2+}, which indicated that these magnetite-encapsulated hematite mineral particles can be recycled by low-intensity magnetic separation.

CRediT authorship contribution statement

Wen-bo LI: Supervision, Project administration, Funding acquisition; **Shao-kai CHENG:** Methodology, Validation, Investigation, Writing − Original draft; **Rui QU:** Data curation, Visualization, Conceptualization; **Ji-jia CHEN:** Supervision, Writing − Review & editing.

Declaration of competing interest

The authors declare that they have no known competing financial interests or personal relationships that could have appeared to influence the work reported in this paper.

Acknowledgments

The authors gratefully acknowledge and appreciate the financial support from the National Key R&D Program of China (No. 2022YFC2905800), and the National Natural Science Foundation of China (Nos. 52174242, 52130406).

References

[1] BALARAM V. Rare earth elements: A review of applications, occurrence, exploration, analysis, recycling, and environmental impact [J]. Geoscience Frontiers, 2019, 10(4): 1285−1303.

[2] CHENG Shao-kai, LI Wen-bo, HAN Yue-xin, SUN Yong-sheng, GAO Peng, ZHANG Xiao-long. Recent process developments in beneficiation and metallurgy of rare earths: A review [J]. Journal of Rare Earths, 2024, 42(4): 629−642.

[3] DUSHYANTHA N, BATAPOLA N, ILANKOON I M S K, ROHITHA S, PREMASIRI R, ABEYSINGHE B, RATNAYAKE N, DISSANAYAKE K. The story of rare earth elements (REEs): Occurrences, global distribution, genesis, geology, mineralogy and global production [J]. Ore Geology Reviews, 2020, 122: 103521.

[4] ZHOU Bao-lu, LI Zhong-xue, CHEN Cong-cong. Global potential of rare earth resources and rare earth demand from clean technologies [J]. Minerals, 2017, 7(11): 203−216.

[5] DUTTA T, KIM K H, UCHIMIYA M, KWON E E, JEON B H, DEEP A, YUN S T. Global demand for rare earth resources and strategies for green mining [J]. Environmental Research, 2016, 150: 182−190.

[6] KUMARI A, PANDA R, JHA M K, KUMAR J R, LEE J Y. Process development to recover rare earth metals from monazite mineral: A review [J]. Minerals Engineering, 2015, 79: 102−115.

[7] ESPIRITU E R L, NASERI S, WATERS K E. Surface chemistry and flotation behavior of dolomite, monazite and bastnäsite in the presence of benzohydroxamate, sodium oleate and phosphoric acid ester collectors [J]. Colloids and Surfaces A: Physicochemical and Engineering Aspects, 2018, 546: 254−265.

[8] MENG De-liang, HUANG Xiao-wei, FENG Zong-yu, WANG Meng, XIA Chao, ZHAO Yan-yan. Thermal decomposition of Bayan Obo mixed rare earth concentrate under inert atmosphere [J]. Transactions of Nonferrous Metals Society of China, 2023, 33(1): 285−292.

[9] JORDENS A, CHENG Ying-ping, WATERS K E. A review of the beneficiation of rare earth element bearing minerals [J]. Minerals Engineering, 2013, 41: 97−114.

[10] HUANG Xiao-wei, LONG Zhi-qi, WANG Liang-shi, FENG Zong-yu. Technology development for rare earth cleaner hydrometallurgy in China [J]. Rare Metals, 2015, 34(4): 215−222.

[11] BISAKA K. Extraction of rare earths from iron-rich rare earth deposits [J]. Journal of the Southern African Institute of Mining and Metallurgy, 2017, 117(8): 731−739.

[12] CHEN Y, HE D, POTGIETER J H. Development and beneficiation technology of rare earth ores in China [J]. Journal of the Southern African Institute of Mining and Metallurgy, 2022, 122(3): 125−132.

[13] ZHANG Qiang, SUN Yong-sheng, HAN Yue-xin, GAO Peng, LI Wen-bo, BAI Zhe. Pyrolysis behavior of bastnaesite in an air environment: Thermodynamics, phase transition and kinetics [J]. Journal of the Taiwan Institute of Chemical Engineers, 2023, 152: 105188.

[14] CHENG Shao-kai, HAN Yue-xin, TANG Zhi-dong, LI

Wen-bo. Producing magnetite concentrate from iron tailings via suspension magnetization roasting: A pilot-scale study [J]. Separation Science and Technology, 2023, 58(7): 1372−1382.
[15] YUAN Shuai, QIN Yong-hong, JIN Jian-ping, LI Yan-jun. Improving vanadium extraction from refractory stone coal by suspension roasting [J]. Transactions of Nonferrous Metals Society of China, 2023, 33(3): 902−916.
[16] NUNNA V, HAPUGODA S, POWNCEBY M I, SPARROW G J. Beneficiation of low-grade, goethite-rich iron ore using microwave-assisted magnetizing roasting [J]. Minerals Engineering, 2021, 166: 106826.
[17] DING Yin-gui, WANG Jing-song, WANG Guang, XUE Qing-guo. Innovative methodology for separating of rare earth and iron from Bayan Obo complex iron ore [J]. ISIJ International, 2012, 52(10): 1772−1777.
[18] YANG He, RONG Yi, TANG Rong, XUE Xiang-xin, LI Yong. Recovery of iron from Baotou rare earth tailings by magnetizing roast [J]. Rare Metals, 2013, 32(6): 616−621.
[19] FARIS N, TARDIO J, RAM R, BHARGAVA S, POWNCEBY M I. Investigation into coal-based magnetizing roasting of an iron-rich rare earth ore and the associated mineralogical transformations [J]. Minerals Engineering, 2017, 114: 37−49.
[20] LI Wen-bo, CHEN Ji-jia, ZHOU Wen-tao, HAN Yue-xin, SHAN Yan. Effect of bastnaesite as reductant on hematite reduction during in-situ suspension magnetization roasting of refractory iron ore under neutral atmosphere [J]. International Journal of Mining Science and Technology, 2022, 32(4): 877−886.
[21] ZHANG Qiang, SUN Yong-sheng, HAN Yue-xin, GAO Peng, LI Wen-bo. Pyrolysis mechanism of bastnaesite during roasting in N_2 atmosphere: An in-situ study of gas products, phase transition, and kinetics [J]. Journal of Industrial and Engineering Chemistry, 2023, 124: 381−391.
[22] CEN Peng, WU Wen-yuan, BIAN Xue. Thermodynamic mechanism analysis of calcification roasting process of bastnaesite concentrates [J]. Metallurgical and Materials Transactions B, 2017, 48(3): 1539−1546.
[23] MOSTAFA A T M G, EAKMAN J M, MONTOYA M M, YARBRO S L. Prediction of heat capacities of solid inorganic salts from group contributions [J]. Industrial & Engineering Chemistry Research, 1996, 35(1): 343−348.
[24] MOSTAFA A T M G, EAKMAN J M, YARBRO S L. Prediction of standard heats and Gibbs free energies of formation of solid inorganic salts from group contributions [J]. Industrial & Engineering Chemistry Research, 2002, 34(12): 4577−4582.
[25] BARIN I. Thermochemical data of pure substances [M]. 3rd ed. Weinheim: Wiley-VCH Verlag GmbH, 1995.
[26] ZHAO Long-sheng, WANG Liang-shi, SHUAI Geng-hong, LONG Zzhi-qi, CUI Da-li, HUANG Xiao-wei. Thermal decomposition and oxidation of bastnaesite concentrate in inert and oxidative atmosphere [J]. Journal of Rare Earths, 2018, 36(7): 758−764.
[27] JORDÁN D, GONZÁLEZ-CHAVEZ D, LAURA D, LEÓN HILARIO L M, MONTEBLANCO E, GUTARRA A, AVILÉS-FÉLIX L. Detection of magnetic moment in thin films with a home-made vibrating sample magnetometer [J]. Journal of Magnetism and Magnetic Materials, 2018, 456: 56−61.
[28] YUAN Shuai, LIU Xiao, GAO Peng, HAN Yue-xin. A semi-industrial experiment of suspension magnetization roasting technology for separation of iron minerals from red mud [J]. Journal of Hazardous Materials, 2020, 394: 122579.
[29] ZHU Xin-ran, HAN Yue-xin, SUN Yong-sheng, LI Yan-jun, WANG Hao-wei. Siderite as a novel reductant for clean utilization of refractory iron ore [J]. Journal of Cleaner Production, 2020, 245: 118704.
[30] YUAN Shuai, XIAO Han-xin, WANG Ruo-feng, LI Yan-jun, GAO Peng. Improved iron recovery from low-grade iron ore by efficient suspension magnetization roasting and magnetic separation [J]. Minerals Engineering, 2022, 186: 107761.
[31] WANG Ruo-feng, YUAN Shuai, GAO Peng, LI Yan-jun. Application of suspension magnetization roasting as technology for high-efficiency separation of valuable iron minerals from high-iron bauxite [J]. Transactions of Nonferrous Metals Society of China, 2022, 32(7): 2391−2402.

悬浮磁化焙烧过程中氟碳铈矿对赤铁矿的原位还原机制

李文博[1,2]，程绍凯[1,2]，瞿 瑞[1,2]，陈继佳[1,2]

1. 东北大学 资源与土木工程学院，沈阳 110819；
2. 难采选铁矿资源高效开发利用技术国家地方联合工程研究中心，沈阳 110819

摘 要：为探究含铁稀土矿在悬浮焙烧过程中的自磁化，以赤铁矿与氟碳铈矿混合矿为研究对象，考察 N_2 气氛下焙烧温度、焙烧时间和氟碳铈矿与赤铁矿质量比对赤铁矿原位还原的影响。采用相关分析检测研究焙烧过程中的矿相演变、焙烧产品的磁性和显微组织、精矿的物相组成及表面元素价态。结果表明，在最佳焙烧条件下，获得铁品位为 68.87%、铁回收率为 93.18%的磁选铁精矿。在焙烧过程中，氟碳铈矿分解生成 CO_2 和 CO，同时赤铁矿的致密结构逐渐被破坏，产生微裂纹。随后，生成的 CO 随着裂隙进入赤铁矿颗粒表层并与其发生反应，形成磁铁矿壳，且这种磁铁矿包裹赤铁矿的颗粒可被弱磁选回收。

关键词：氟碳铈矿；赤铁矿；磁化焙烧；原位还原

(Edited by Xiang-qun LI)